Applied Catalysis B: Environmental 244 (2019) 250–261

Contents lists available at ScienceDirect

Applied Catalysis B: Environmental

journal homepage: www.elsevier.com/locate/apcatb

Dehydration of fructose over thiol– and sulfonic– modified alumina in a continuous reactor for 5–HMF production: Study of catalyst stability by NMR

Francisco Jose Morales-Leal[a], Javier Rivera de la Rosa[a,*], Carlos J. Lucio-Ortiz[a], David A. De Haro-Del Rio[a], Carolina Solis Maldonado[b], Sungsool Wi[c], Leah B. Casabianca[d], Carlos D. Garcia[d]

[a] Universidad Autónoma de Nuevo León, UANL, Facultad de Ciencias Químicas, San Nicolás de los Garza, Nuevo León, 64450, Mexico
[b] Universidad Veracruzana, Facultad de Ciencias Químicas, Prolongación Venustiano Carranza S/N, Poza Rica, Veracruz, 93390, Mexico
[c] National High Magnetic Field Laboratory, Florida State University, Tallahassee, FL, 32310, USA
[d] Clemson University, Department of Chemistry, Clemson, South Caroline, 29634, USA

ARTICLE INFO

Keywords:
Fructose
5–HMF
Modified alumina
DNP-NMR
Grafting

ABSTRACT

In the present study, the synthesis of an organic group–modified alumina by the sol–gel method is proposed. This material has shown to have an enhanced catalytic performance with grafted organic groups and showed an improved stability. The prepared material has shown to have several O—H groups and an enhanced surface acidity. The alumina acidity was improved by incorporating thiol groups by grafting method, which promotes the tautomerization of fructose to its furanose form. Furthermore, the grafting of sulfonic groups catalyzes its dehydration. The modified alumina was thermally treated up to 200 °C to improve the functional groups stability. After, this modified material was packed into a continuous reactor system, designed and built by this group, to obtain 5–hydroxymethylfurfural (5–HMF) from fructose dissolved in a single–phase solution of tetrahydrofuran (THF) and H_2O (4:1 w/w). The catalytic activity of this material was evaluated by the reaction of fructose dehydration at different reaction temperatures (60, 70, 80 and 90 °C). Fructose conversion and selectivity towards 5–HMF were determined by high performance liquid chromatography (HPLC), obtaining 95% and 73% respectively for the highest temperature. The catalyst showed an efficient stability after 24 h in continuous flow at 70 °C. The loss of sulfur content was 15%, but the fructose conversion yield and the selectivity to 5–HMF after 24 h of continuous reaction did not undergo significant changes (less than 5%). The nuclear magnetic resonance (NMR) tests confirmed the presence of the thiol and sulfonic groups before and after 24 h of reaction, as well as the conservation of the same structure, demonstrating the efficient catalytic performance of the material. The catalysts were characterized by nitrogen adsorption/desorption, X–ray diffraction and infrared (IR) spectroscopy. Also, before and after use by utilizing elemental analysis and $^{1}H–^{13}C$ cross–polarization magic–angle spinning (CPMAS) and dynamic–nuclear polarization (DNP)–enhanced $^{1}H–^{13}C$ and $^{1}H–^{29}Si$ CPMAS as well as directly excited ^{29}Si magic–angle spinning (MAS) NMR methods in solid–state.

1. Introduction

The need to create sustainable technological processes that use renewable raw materials, minimization of the use of energy and toxic emissions generated during the process is the goal of many research groups globally. In this way, it is desirable to convert waste streams into valuable chemicals and materials with high market attractiveness through advanced recycling approaches [1,2]. The large amount of waste from existing industrial sectors (e.g., food industry, pulp and paper industry, biodiesel and bioethanol production, etc.) [3] can become an uncharted opportunity to turn the waste into a potential feedstock for the production of sugar–based products to replace petro–chemicals [4,5]. In addition, the homogenous nature of the waste presents an advantage in production of high–purity products via biological or chemical methods, such as, saccharification, adsorption, ion exchange, isomerization, evaporation, etc. [6].

Currently, the development of new catalysts plays a central role in the industry in many aspects, including the efficiency of the processes

* Corresponding author at: Universidad Autónoma de Nuevo León, UANL, Facultad de Ciencias Químicas, San Nicolás de los Garza, Nuevo León, 64450, Mexico.
E-mail address: javier.riverad@uanl.edu.mx (J. Rivera de la Rosa).

https://doi.org/10.1016/j.apcatb.2018.11.053
Received 22 August 2018; Received in revised form 12 November 2018; Accepted 17 November 2018
Available online 19 November 2018
0926-3373/

that are involved in obtaining and saving energy which in turn is a friendly technology environment [7]. In this regard, the design of catalysts with suitable properties for a specific application and catalytic reactions in which wastes are converted to useful products are paramount. Alumina (Al_2O_3) is one of the transition metals oxides that commonly had been used as a platform for the mechanical support and catalytic reactions [8,9]. It has been suggested that the activity of the alumina can be greatly enhanced by introducing functional groups such as hydroxyl, carboxyl, amino, etc., that can be immobilized onto the surface of the catalytic material. Therefore, there have been numerous efforts in adding some target functional groups through diverse grafting methods on the catalytic surface [10].

5–hydroxymethylfurfural (5–HMF) is one of the desired fructose derivates. It is a versatile intermediate molecule, which could be used as chemical platform due to its high reactivity and polyfunctionality that is originated from the furan nature in its structure and the presence of alcohol and aldehyde groups [11]. 5–HMF has been proposed to be used as a feedstock for the synthesis of a wide variety of supplies including pharmaceuticals, polymers, resins, solvents, and biofuels [12]. In addition, 5–HMF plays a significant role in the context of sustainable development, being a product that can be obtained from renewable sources, whose derivatives can replace compounds and materials that have been obtained from petroleum [7,8]. 5–HMF also possesses potential applications in the field of sustainable technologies to produce polymers and biofuels [13]. Thus, based on its enormous potential applications in the chemical industry and in the energy sector, it has been considered that the 5–HMF is indeed a "sleeping giant" [14].

5–HMF can be obtained by the dehydration of fructose, glucose and sucrose in the presence of acid catalysts. Some mineral catalysts, such as HCl, H_2SO_4 and H_3PO_4, that have been used normally show a selectivity value up to 50% toward 5–HMF from fructose, with 50% conversion [15]. The incorporation of functional groups as sulfonic acids and thioether groups in mesoporous materials as silica have shown conversion and selectivity values of 80 and 70% respectively to convert fructose into 5–HMF [16]. Also, the 5–HMF production in a batch reactor is well–documented, but there have been relatively a few reports on its continuous production [17]. The continuous dehydration of mono– and polysaccharides to 5–HMF was reported in a biphasic solvent system using titanium or zirconia as the catalyst [18]. Although the titanium was deactivated, it was regenerated by calcination (the regeneration of the zirconia catalyst was not discussed). Unfortunately, the rate of 5–HMF production was not reported as a function of time–on–stream, so the rates of deactivation are unknown. H–mordenite was tested in a continuous pilot plant reactor but catalyst stability was not reported [19,20]. Several niobium–based catalysts were employed for the dehydration of aqueous fructose in a fixed–bed reactor [21–23]. Mixed silica − niobia oxides showed stable activity for ~95 h on–stream at 373 K, despite coke formation, although 5–HMF selectivity was low (< 15%, at fructose conversions from 15 to 35%) [24].

Furthermore, the research conducted by Tucker et al, [18] assessed the activity, selectivity and stability of various acid catalysts such as silica SBA–15 to continuously produce 5–HMF in a reactor from dissolved fructose in a solution of tetrahydrofuran (THF) and water. They found that catalysts with structures containing ordered pores are more selective and stable than those containing unordered pores. Moreover, the stability of the catalysts of mesoporous silica functionalized with propyl sulfonic acid depends both on the solvent system and temperature; the absence of an optimal combination of both generates a loss in the catalyst activity, which can be caused by cleavage of the active sites of the support, blocking access to the active sites or deposition of products in insoluble reaction pores. Finally, they found that the stabilities of the silica catalysts based on organosilica should be evaluated in the demanding conditions typically required for efficient conversion of biomass (elevated temperature range, 50–500 °C, and high–water content) [18]. However, the disadvantage presented in this investigation is attributed to the deactivation of catalytic activity in the modified catalyst, the loss of grafted functional groups was mainly generated by hydrolytic cleavage of the active sites [15,16].

There has been no detailed investigation of the stability of solid acid catalysts achieving a high selectivity to 5–HMF [18]. Hence, the purpose of this work is to achieve superior catalytic stability using synthetic surface–modified alumina. For this, alumina by the sol–gel method was synthesized, and a thiol and sulfonic groups were grafted on it for the dehydration of fructose and evaluate the selectivity rates in the 5–HMF formation. Moreover, factors such as temperature and solvent system during the catalyst synthesis (sol–gel and grafting methods) and reaction processes were controlled [23,25]. The novelty of this work is the design and use of this bifunctional catalyst in a continuous reactor system and the stability of the catalyst has been studied by solid-state NMR spectroscopy.

2. Experimental Methods

2.1. Reagents and materials

Aluminum tri–sec–butoxide (ATB, 97%), NaH (dispersed in mineral oil, 60%), toluene, ethanol (99.5%), fructose (≥99%), 3–mercaptopropyl–trimethoxysilane (MPTMS, 95%), 2–butanol (2–ButOH, 99.8%), 1,3–propanesultone (PST, > 99%), hexane (95%), ethyl acetate (99.9%), tetrahydrofuran (THF, 99.9%), HCl 37% and ethyl ether 99.99% were purchased from Sigma and used as received. Methanol 99.98% was obtained from JT Baker. For comparative purposes, commercial alumina SBA–CATALOX 200 was purchased from Sasol and used as received. 0.5 M ethereal HCl was prepared to add 4.9 g of HCl, 2.03 mL of methanol and gauged to 100 mL with ethyl ether. Deionized and nanopure water was obtained by a PURELAB CLASSIC, Elga brand, model Classic UVF. The alumina catalysts synthesized for this work were dried at atmospheric pressure at 200 °C for 24 h and stored in a glovebox prior to characterization. Previously to reaction studies, the catalysts were stored in a desiccator to prevent adsorption of atmospheric moisture.

2.2. Characterization

The characterization of the materials was conducted via X–ray diffraction (XRD) using a Siemens X–ray equipment (model D5000, series E04–0012). The parameters were as follows: the scale of 2 Theta, with Ni–filtered Cu Kα radiation, starting at 5° and finishing at 90°, step size of 1.4°, time per step of 1 min, and temperature of 25 °C. FTIR–ATR spectroscopy patterns were collected from 500 to 4000 cm^{-1} (wavenumber), using a Perkin–Elmer, model Spectrum One. Computational FTIR simulation was done to detect characteristic bands of 5–HMF, THF and fructose, because in solution the characteristic bands of the 5-HMF are transposed with those of the THF and fructose. For this, the molecules were built and pre–optimized in Avogadro v. 1.0. Then, they were transferred to Gabedit v. 2.4.8 for structural optimization and calculation of their vibrational frequencies through MOPAC2016 and the Hamiltonian PM7. All the optimal structures had real frequencies. Gabedit was also used to visualize the results of the MOPAC2016 calculation and to generate the simulated IR spectra, by adjusting Lorentz peaks at the frequencies reported by MOPAC2016. N_2 adsorption/desorption measurements were performed on an AUTOSORB–1 Quantachrome Automated Gas Sorption System Report. The point zero charge of spent ASB catalyst was developed using the method reported by Yun et al. [20]. 50 mg of spent ASB catalyst were placed in 50 mL containers. By other hand, 21 solutions were prepared at specific pH values using solutions of HNO_3 0.1 M and standard NaOH 0.1 M and NaCl 0.1 M. 25 mL of each solution was added to the flasks containing the spent ASB catalyst and were subjected to constant agitation of 250 rpm for 48 h at 25 °C. After 48 h were elapsed, the pH of the samples and the target were measured. DNP–enhanced ^{1}H–^{29}Si and ^{1}H–^{13}C

CPMAS and directly polarized ^{29}Si MAS NMR spectra were recorded on a wide–bore 600 MHz Bruker Avance III spectrometer and 395 GHz gyrotron system equipped with a triple resonance 3.2 mm MAS probe. The sample temperature for DNP experiments was maintained at about 100 K. DNP–enhanced ^{1}H–^{13}C and ^{1}H–^{29}Si CPMAS NMR spectra were acquired after optimizations by employing a saturation recovery pulse along the proton channel. For both cases, the optimal build–up times was about 10 s. Typically, 256 scans were acquired at a spinning rate of 8 kHz. Chemical shifts were referenced using tetrakis–(trimethylsilyl) silane. Two different type of DNP sampling conditions were utilized to diagnose samples in different polarities. Under the hydrophilic sampling condition, about 20 mg of each sample was mixed with 20 µL of 1–(TEMPO–4–oxy)–3–(TEMPO–4–amino)propan–2–ol (TOTAPOL, where TEMPO is 2,2,6,6–tetramethylpiperidine–1–oxyl) 5 mM in 90% D_2O and 10% H_2O for ^{1}H–^{13}C CPMAS NMR spectroscopy and about 20 mg of each sample was mixed with 20 µL of nitroxide biradical AMUPol 10 mM in 78% DMSO–d_6, 14% D_2O, and 8% H_2O for ^{1}H–^{29}Si CPMAS and directly excited ^{29}Si MAS NMR spectroscopy. Under the hydrophobic condition about 20 mg of each sample was mixed with 20 µL of dinitroxide radical TEKPol 15 mM in 90% tetrachloroethane (TCE) and 10% DMSO–d_6 for ^{1}H–^{29}Si CPMAS and directly excited ^{29}Si MAS NMR spectroscopy. Each sample mixture was pack into a 3.2 mm zirconia rotor with a vessel cap for low–temperature experiments. Conventional ^{1}H–^{13}C CPMAS NMR spectroscopy at room temperature was carried out on a wide–bore 500 MHz Bruker Avance III spectrometer equipped with 2.5 mm MAS probe. Typically, about 26,000 scans were acquired for obtaining a ^{1}H–^{13}C CPMAS spectrum at room temperature at a spinning rate of 10 kHz. Chemical shifts were referenced using tetrakis–(trimethylsilyl)silane. Elemental analysis was performed by Antlatic Microlab, Inc. (Norcross, GA).

2.3. Synthesis of alumina by sol–gel method

In a three–necked reactor 2–ButOH was added and brought to a temperature between 90 and 95 °C. Then, ATB was added under stirring and refluxed for 2 h. The system was brought to room temperature, and deionized water was added and stirred for 2 h to obtain a clear gel. The gel was transferred to a beaker and allowed to age at room temperature for 24 h. The formed gel was dried at 110 °C for 24 h. Finally, the xerogel obtained was calcined at 500 °C for 6 h in order to obtain a very stable support with enough OH– available groups on the surface to the functionalization process [8,17]. The molar ratios were as follows: 2–ButOH / ATB (60:1), H_2O / ATB (1:1) [15,23]. The material obtained was labeled as AS.

2.4. Modification of synthetic alumina with organic acid groups by grafting method

A) Thiol group: 1.5 g of the AS were taken and suspended in 50 mL of toluene; after 0.9 mL (4.60 mmol) of MPTMS and allowed to stir at reflux for 36 h was added. The mixture was filtered, and the solid obtained was washed three times with 15 mL of ethanol [15,23]. Finally, it was dried at 200 °C in a muffle furnace for 12 h. The synthesized functionalized alumina was labeled as ASF. **B) Sulfonic group:** under conditions of N_2 flow in a three–necked flask precooled to −78 °C, 25 mL of THF was added and 1 g of ASF catalyst. Moreover, a suspension of NaH in THF (400 mg / 15 mL) was added slowly to the flask. It was allowed to stand 30 min, and then 1.3 mL (14.52 mmol) of PST was added and allowed to stir about 18 h while the flask reached room temperature. The reaction was quenched with 50 mL of deionized water then filtered. The solid collected was washed three times with 25 mL of hexane and 25 mL of ethyl acetate, then washed with 25 mL of 0.5 M ethereal HCl and 75 mL of methanol [15,23]. Finally, the solid was dried at 200 °C in a muffle furnace for 12 h. The bi–functionalized catalyst was identified as ASB. In Fig. 1, can be shown the expected mechanism after alumina synthesis and modification.

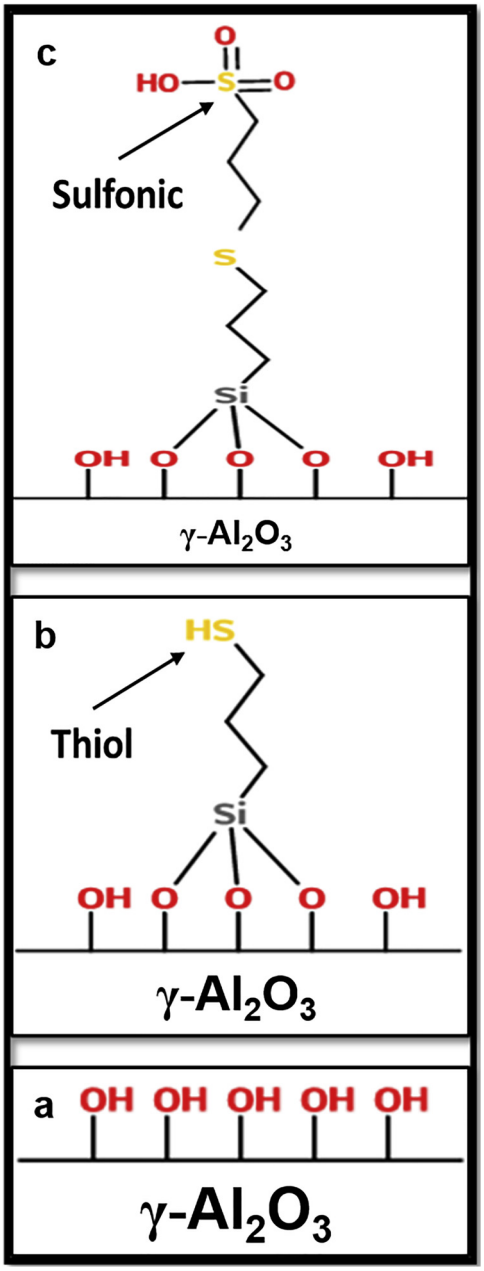

Fig. 1. Synthesis and modification of alumina catalysts by (a) sol–gel method, (b) grafting method with thiol group (functionalization) and (c) grafting method with sulfonic group (bi–functionalization).

2.5. General procedures for continuous fructose dehydration

The reaction was carried out at the conditions reported by Tucker et al. (2012), who have reported the highest conversion and selectivity to 5–HMF from fructose in continuous processes [18]. The reaction was developed in a continuous fluidized bed reactor of 316 stainless steel schedule 10 and 1/4" diameter (Hoke) connected with 0.5 µm filter (Swagelok) at the ends to prevent entrainment of the catalyst in the system. In this, they have placed 500 mg of catalyst (ASB) and heated up with an electric furnace between the temperatures of 60–90 °C, in which tests the steady state for the determination of conversion and selectivity were performed. During tests, it was observed that the steady state was reached after 3 min of obtaining the reaction products. The reactor was passed a solution of fructose which consisted of dissolving 2% by weight of fructose in a mixture of THF and nanopure water (Type I) in a 4:1 w/w respectively, through an HPLC pump, driving a

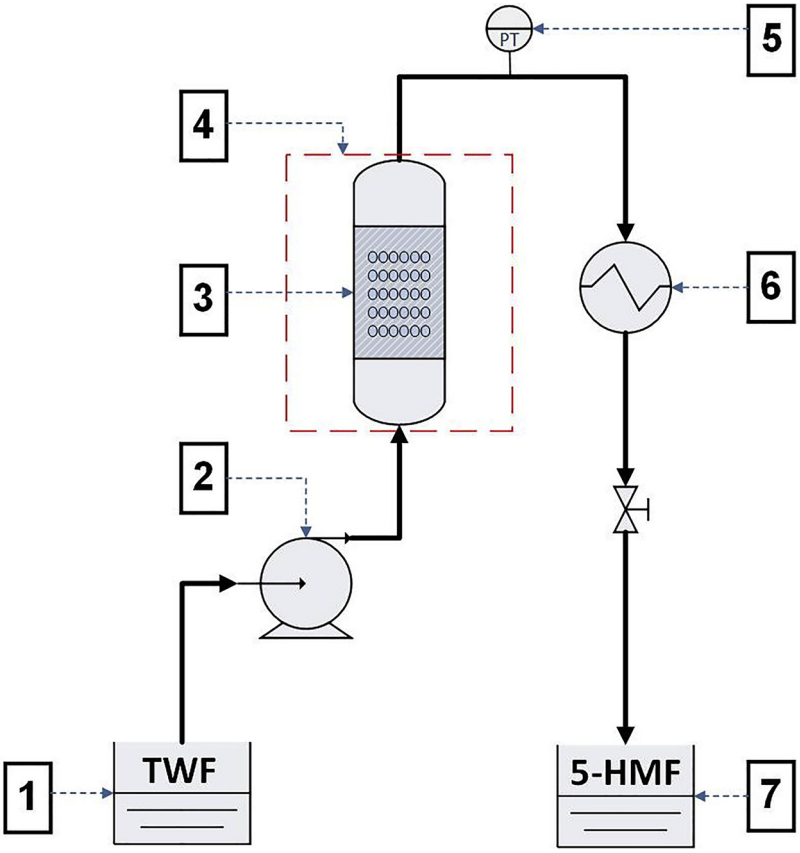

Fig. 2. Schematic representation of fructose catalytic dehydration process in a continuous reactor, where: (1) liquid feed which consisted of dissolving fructose (2 wt.%) in a mixture of THF–water 4:1 w/w, (2) HPLC pump driving a volumetric flow of 1 mL*min^{-1}, (3) ¼" diameter reactor loaded with ASB pure catalyst and 0.5 µm stainless porous disk at the extremes, (4) reactor heating zone, (5) pressure and temperature meter, (6) cooler and (7) reaction products measured by HPLC.

volumetric flow of 1 mL*min^{-1}, a contact time with the catalyst bed of 0.5 g*min*mL^{-1} and a Liquid Hourly Space Velocity (LHSV) of 2 mL*min^{-1}*g^{-1}. After the reaction was complete, the product was obtained by a cooling bath to prevent boiling of the mixture (Fig. 2). The employed furnace during heating was brand SASABE, 8/9 Fusion model. The pump used was HPLC–Class M1, Chrom Tech brand, model LC10 SS SF DRS NPD FB–10. The nanopure water was obtained by a PURELAB CLASSIC, Elga brand, model Classic UVF. During the reaction, the product stream was analyzed using a Waters e2695 HPLC system. Fructose and 5–HMF were analyzed using an Aminex HPX–87 P column (Biorad) held at 358 K, with Milli–Q water as the mobile phase at a flow rate of 0.6 mL min^{-1}. Fructose concentration was monitored using a Waters 2414 refractive index detector, and 5–HMF concentration was determined using a Waters 2998 photodiode array detector at 320 nm. Fructose conversion was calculated as moles of fructose reacted per mole of fructose–fed. 5–HMF selectivity was calculated as moles of 5–HMF produced per mole of fructose reacted.

3. Results and discussion

3.1. Characterization of alumina support by XRD

Fig. 3 shows the X–ray diffraction pattern of the alumina support synthesized by sol–gel method, starting from the precursors ATB and 2–butanol as solvent [8], calcined at different temperatures. Similarly, to ensure the similarity of the samples with a standard, a sample of commercial alumina (AC) brand CATALOX® SBa–200 Sasol was run, which was duly identified according to the JCPDS card No. 00–029–0063 of the γ–alumina phase, whose arrangement is cubic centered on the faces [26].

According to Fig. 3, it can be observed how the X–ray diffraction pattern in the four samples shows peaks with intensities centered at 37°, 46° and 67°, characteristics of the γ–alumina [27] related to the planes (311), (400) and (440) respectively [28]. It can also be observed that the greater the degree of heat treatment applied on the synthetic alumina supports, the greater the degree of crystallinity, evidence of which is the greater intensity of the peaks. Obviously, commercial alumina is much more crystalline because it is calcined at temperatures around 1000 °C [29], which indicates a much more crystalline arrangement.

3.2. Characterization of alumina catalysts by FTIR

In order to monitor the grafted functional groups on the alumina after modification, in Fig. 4 the infrared spectra of commercial alumina (AC), synthetic alumina (AS), functionalized synthetic alumina (ASF) and bi–functionalized synthetic alumina (ASB) are shown.

In Fig. 4, the band at 3473 cm^{-1} is related to the vibrations of O—H groups, which are more intense in AS than in AC. These results were expected since the sol–gel synthesis method favors a greater amount of O—H groups, and because at low calcination temperatures favor low loss during dehydroxylation of O—H groups. This feature is important because the O—H groups favor the grafting of the thiol group [17]. It is evident that the modified catalysts have bands around 2853 cm^{-1} related to vibrations stretching symmetrical and asymmetrical of the methyl C—H (CH_3 and CH_2) bonds, which indicate the presence of the propyl group from MPTMS, observed in ASB more intensely due to the presence of the propyl group from 1,3–propanesultone [30]. Also, a very small band around 2570 cm^{-1}, which corresponds to thiol group (S—H) bonds, was observed and virtually disappeared when bi–functionalization was carried out with sulfonic acid groups (SO_3H) [31]. This bi–functionalization gave rise to the appearance of new bands around 1043, 1146, and 1198 cm^{-1} relating to the grafted sulfonic acid groups [14,15].

Therefore, when the functionalization with MPTMS was carried out, the C—H band of the propyl group from MPTMS was more intense in the ASF spectrum and thus decreased the O—H band compared to AS,

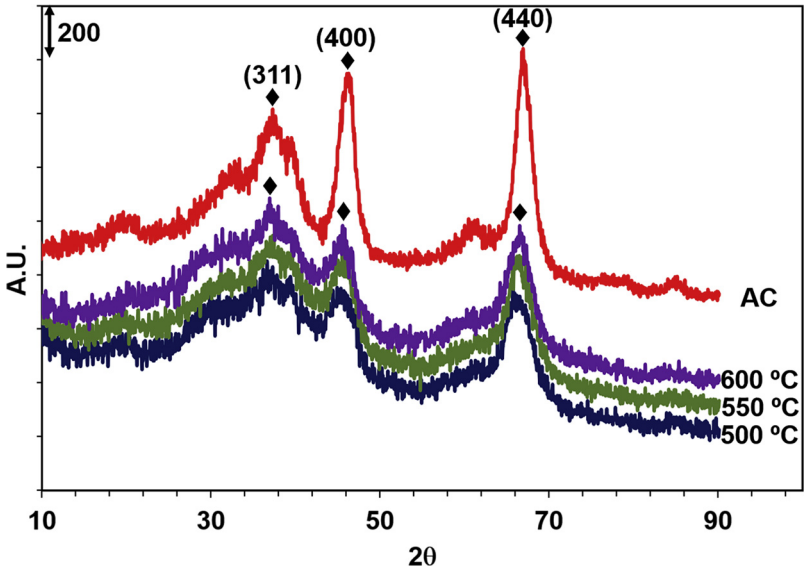

Fig. 3. Comparison between X–ray patterns of commercial alumina (AC) and supports of synthetic alumina (AS) calcined at different temperatures (500, 550 and 600 °C). Phase γ–alumina (♦).

which means there is a greater amount of the functionalized group. In addition, the band at 1035 cm^{-1} in ASF is related to the symmetric and asymmetric stretching of sulfonated groups which are partially transposed with the vibrations of the silane group (Si—O) [32]. After bi-–functionalization with sulfonic groups, which bind to the S—H groups available at the surface, the intensity of the band at 2570 cm^{-1} is said to decrease [33]. It should be noted that not all S—H groups are occupied by sulfonic acid groups, some are free. Related bands were more intense for sulfonic groups in the ASB catalyst because this one had a high quantity of S—H groups available to be grafted by sulfonic. Furthermore, it is also seen that the intensity of the O—H band increases, due to O—H stretching in sulfonic acid, silanol, and remaining water groups [34–37]. The band at 850 cm^{-1} is attributed to tetrahedral Al—O stretching [35,36].

3.3. Textural properties of the catalysts under study by BET and BJH methods

The samples were analyzed by using nitrogen adsorption/desorption isotherms at 77.4 K, and isotherms were calculated by multipoint BET method (Brunauer–Emmet–Teller) surface area and the BJH method (Barrett–Joyner–Halenda) the volume and pore size. The results of the AC, AS and ASB catalysts are shown in Table 1. Accordingly, the alumina catalysts synthesized by sol–gel have higher surface area and pore volume than commercial alumina, which is more favorable for the catalytic activity of this material in the reaction process under study, which is supported by the literature [37,38]. Moreover, when transition alumina undergoes processes of calcination at higher temperatures, significant growth of the primary particle is produced due to small and continuous structural rearrangements of aluminum ions, which is evidenced by decreasing BET surface area [39–41]. In the same

Table 1
Textural properties of studied catalysts.

Catalyst	Surface Area BET (m^2/g)	Pore Diameter BJH (nm)	Pore Volume BJH (cc/g)	Pore Classification (IUPAC)
AC	199.1	6.12	0.40	Mesopores
AS	375.4	6.12	2.16	Mesopores
ASB	142.1	4.62	0.80	Mesopores

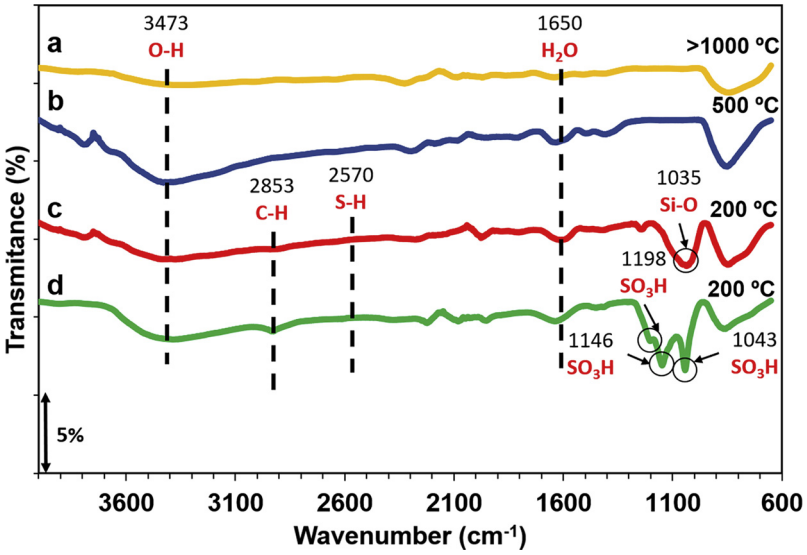

Fig. 4. FTIR spectra of: (a) commercial alumina (AC, yellow line), (b) synthetic alumina (AS, blue line), (c) functionalized catalyst with thiol groups (ASF, red line) and (d) bi–functionalized catalyst with thiol and sulfonic groups (ASB, green line) (For interpretation of the references to colour in this figure legend, the reader is referred to the web version of this article).

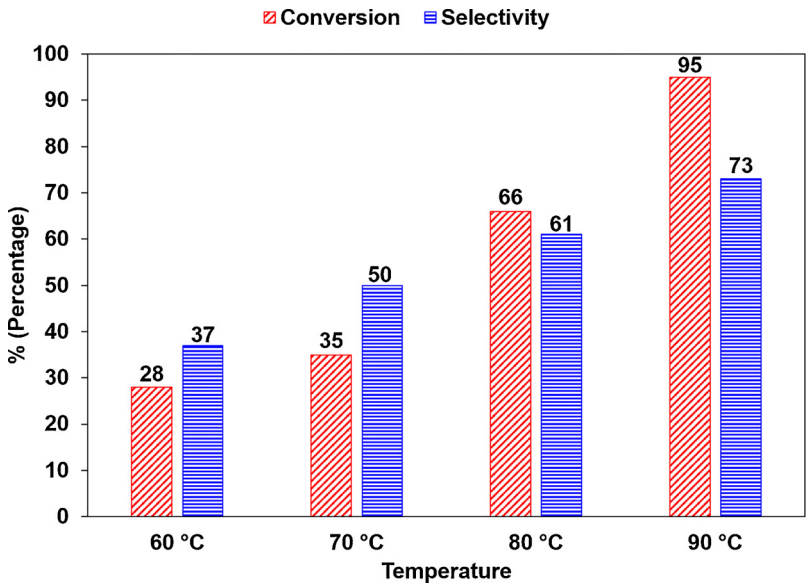

Fig. 5. Fructose conversion (diagonal stripes) and selectivity towards 5–HMF (horizontal stripes) at different reaction temperatures.

way, it is seen that the incorporation of organic groups decreased surface area from 375.4 m^2/g (catalyst AS) to 142.1 m^2/g (catalyst ASB), which may be due to the organic groups changing the properties of alumina, such as acidity [17], resulting in a lower specific surface area, during grafting. Moreover, as these groups are grafted on the catalyst surface, available sites were occupied taking place the same phenomenon. Similarly, it was found that the pore volume and average pore diameter also decreased for the catalyst ASB, which can relate to the above, in that the organic groups incorporated by grafting may be deposited on the catalyst surface covering the mesopores and leaving available macropores.

3.4. Catalytic activity

Fig. 5 shows the conversion of fructose and selectivity to 5–HMF percentages in the presence of alumina modified catalyst (ASB) at different steady–state reaction temperatures. According to the results in Fig. 5, the conversion of fructose is higher as reaction temperature increases, in such a way that when the temperature reaches 90 °C, the fructose results in a steady state conversion of 95%. The same behavior occurs with the selectivity to 5–HMF, since as the temperature increases the selectivity also increases. Reaching a value of 73% when the reaction temperature is 90 °C.

On the other hand, in this work the rate of reaction and the rate of 5–HMF production as initial TOF (turnover frequency, measured under steady–state conditions) were 2.97×10^{-4} mol/s–g_{cat} and 0.2 s^{-1} respectively. In this regard, Tucker et al, reported the rate of reaction and initial TOF values of 6.34×10^{-5} mol/s–g_{cat} and 0.091 min^{-1} (1.52×10^{-3} s^{-1}) respectively [18], in which it can be observed that the rational surface modification of the ASB catalyst significantly improved the activity of the "active" site, which explains the increase in conversion and selectivity (see Table 3). For this work, the reaction rate was calculated using the next equation, $-r'_A \cong F_{A0} \times x/W$, where F_{A0} is the inlet molar flow of 5–HMF (in mol/s), x is the conversion fraction (dimensionless), and W is the weight of catalyst (in grams). Also, the turnover frequency was calculated as $TOF = -r'_A/S$, where S is the number of active sites (in mol/g). The number of active sites was estimated from the experimental initial amount of sulfur contained in the catalyst and obtained from elemental analysis of sulfur [18,26] (see Table 4).

Due to our laboratory facilities, the tests were performed at atmospheric conditions at the outlet of the reactor, and it was not possible to carry out tests at higher reaction temperatures since solvent system boils and the fructose caramelizes from 90 °C, but other authors have conducted the dehydration of fructose at higher pressure [24,25,41,42]. Furthermore, according to the analysis and despite limitations, the values obtained in this work (fructose conversion and selectivity to 5–HMF) at 90 °C are comparable with the current values of the literature in the scientific community worldwide [16–18] (see Table 3).

3.5. Monitoring the reaction by FTIR

To demonstrate the formation of 5–HMF during the reaction, aliquots were taken at steady state analyzed by FTIR and compared with a target of tetrahydrofuran–water–fructose (TWF) system without the presence of 5–HMF. Fig. 6a and b show the spectra of the analysis. According to results shown in Fig. 6a, it can be seen in the TWF system O—H group band at 3385 cm^{-1} due to stretching vibrations of these groups in fructose and water [43]. This band increases its intensity at the higher reaction temperature, which can be explained by the stretching vibrations of the O—H bond present in the alcohol group of the molecule 5–HMF, indicating the presence of the latter in the products [24]. It can also be observed at 2980 and 2877 cm^{-1} the presence of two characteristic peaks of THF, due to the vibrations of C—H asymmetric stretching, it is noted that while increasing the reaction temperature these are decreasing, which is explained by THF being a volatile compound, the concentration decreases at higher temperatures, demonstrating the decrease in the bands [44].

Moreover, it is also apparent the 1650 cm^{-1} characteristic peak transposes between C—C bonds, the torsional vibration of THF, and the C═O stretching vibrations (aldehyde) of 5–HMF, forming a single peak [24,44]. Note, that said peak intensity increases with increasing reaction temperature, this is because as the THF concentration lowers, the peak increases due to an increase in the 5–HMF concentration in the product. Furthermore, 1522 cm^{-1} shows a small band due to C═C stretching vibrations from the 5–HMF ring in the molecule [24]. Significantly, this small band is not observed in the spectrum of the TWF system but begins to appear in the spectra of the reaction product and start becoming more noticeable as the temperature increases, which clearly indicates, again, the appearance of 5–HMF in the reaction products and its increase in concentration. Fig. 6b shows a *zoomed* image of Fig. 6a between 1700 and 1500 cm^{-1}, in order to observe more detail as the 1650 cm^{-1} band, from C═O vibrations stretching of the aldehyde group in the 5–HMF, and the band at 1522 cm^{-1}, due to C═C stretching

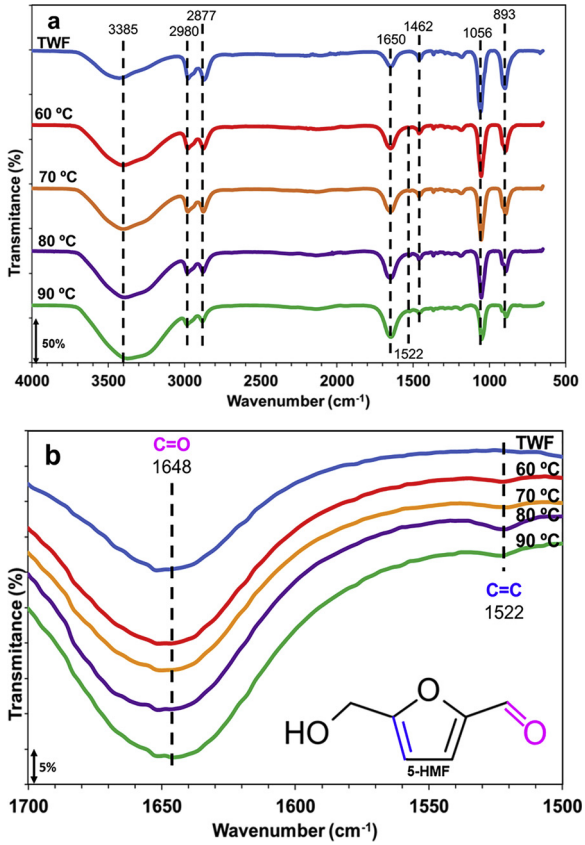

Fig. 6. FTIR spectra of the reaction products at different temperatures, where (a) scanning from 500 to 4000 cm^{-1} and (b) scanning–zoom from 1500 to 1700 cm^{-1}. TWF is tetrahydrofuran–water–fructose system.

Table 2
Vibrations of the bonds in the reaction product species analyzed in FTIR.

Wavenumber (cm^{-1})	Molecule		
	5–HMF [24]	Fructose [43]	THF [44]
3385	υ(O–H)	υ(O–H)	————
2980	υ(C–H)	————	υ_{as}(C–H)
2877	υ_{as}(C–H)	υ(C–H)	υ_{as}(C–H)
1650	υ(C = O)	————	τ(C–C)
1522	υ(C = C)	————	————
1462	————	————	υ_{s}(C–H)
1056	————	υ_{as}(C–O)	υ_{as}(C–O)
893	————	τ(C–C)	υ_{s}(C–O)

Bonds were obtained from computational FTIR simulation in Avogadro v. 1.0 and Gabedit v. 2.4.8 software's and compared some of them with reported references.

vibrations of 5–HMF ring in molecule, increases [24]. Finally, it can be observed 3–stripes on fructose and THF decreasing intensity at higher reaction temperature, including: at 1462 cm^{-1} vibrations C—H symmetric stretching of THF, at 1056 cm^{-1} vibrations C—O asymmetrical stretching of THF and C—O asymmetric stretch of fructose, and 893 cm^{-1} vibration C—O symmetric stretching of THF and torque C—C fructose [43,44]. These bands are decreasing in intensity because fructose is consumed in the reaction and the THF is volatilized due to reaction temperatures. It is important to mention that all FTIR data is in agreement with the HPLC data related to the detection of fructose, THF and 5-HMF. Table 2 summarizes the band assignments for each of the species analyzed.

3.6. Stability tests

In order to observe ASB catalyst stability over time, tests were performed on the continuous reaction system operating for 12 h at 70 °C, because at 90 °C after two hours of running the reactions is possible to begin the caramelization phenomena of fructose and the line of the continuous reactor can be blocked and to have low safety conditions. Fig. 7 shows the results of that test. The conversion and selectivity behavior remain almost constant over time, presenting small and insignificant falls. This result shows that for a continuous 24–hour reaction conversion and selectivity drop is less than 5%, which shows the efficient stability of the ASB catalyst. It is remarkable, that silica catalyst designed by Tucker et al., which for the first 10 h of activity had a drop in the conversion of 15% approximately. However, the catalyst presented the entrainment of the grafted groups, therefore, they needed to install a silica–gel bed at the exit of the reactor in order to capture the released functional groups [18]. In the case of the batch reactor systems used for the production of 5–HMF at 180 °C, it is important to mention that the conversion and selectivity are favored since a pressurized system of the solvent system is formed in the closed reactor that favors the reaction because it allows that solvent system does not vaporize the medium or that the fructose to these conditions caramelize. That is why, it can be confirmed that the method of modification of alumina synthesized by sol–gel, with these same organic groups, gives this material better catalytic properties compared with other previous works, and performed efficiently in the process of dehydration of fructose as shown in Table 3. The increase in selectivity of 5–HMF compared to other works is due to a bifunctional effect from the surface modifier, since the thiol group is in charge of the tautomerization of the fructose to pyranose form, and according to Scott group, this is the major factor of this increase [16]. Even the catalyst lost 15% of sulfur in 24 h, showing a better stability than other similar catalyst in continuous reactor [18].

3.7. Point of zero charge

Fig. 8 shows the Point of Zero Charge (p.z.c), obtained by potentiometric titration of spent catalyst, which is around pH 8.2, which indicates the presence of OH– groups from alumina and sulfonic group grafted on it. Ozawa et al analyzed the p.z.c of several oxide compounds among them alumina, in which they determined that the measured data of p.z.c for alumina were 8.4, since alumina shows both acidic and basic properties on the surface site due to its specific adsorption of OH − and H + [45]. In a previous work the acid sites characterization was conducted by desorption of pyridine using FT–IR technique (DPFT) and TPD–NH_3 where it was shown that modified alumina catalyst with thiol and sulfonic groups had stronger Lewis acid sites where the concentration of medium–strength acid sites was higher than commercial alumina catalyst [17]. It is essential to develop the catalytic tests of the ASB catalyst without adsorption interaction, but this could be carried out for other phenomena such as Van der Waals forces and hydrogen bridges among others.

3.8. Elemental analysis of fresh and spent catalysts

By contrast, to confirm the stability property of the modified alumina catalyst and thus, establish the relationship between aggregate quantities of precursors for grafting, and quantities of grafted functional groups, an elemental analysis of the ASF and ASB fresh catalysts and ASB spent 12 h and 24 h of continuous reaction at 70 °C was performed. As it is shown in Table 4, for the fresh ASF catalyst, after all the functionalization methodology only 65.6% was grafted, contrary to the expected amount, while for the fresh ASB catalyst 52.9% of grafting was achieved. The methodology in the bi–functionalization is a bit more complex due to the required deprotonation of the sulfonic acid group before grafting, and the amount of solvents used during washing to

Table 3
Comparison of catalysts studied by catalytic researchers in the conversion of fructose to 5–HMF.

Catalyst	Reactor	Reaction temperature (°C)	Conversion[a] (%)	Selectivity[b] (%)	LHSV[c] (ml/min–g_{cat})	Reaction rate[d] (mol/s–g_{cat})	TOF[e] (s^{-1})
Modified SBA–15 (Crisci et al) [16]	Batch	180 (time 30 min)	66	74	—	—	—
Modified alumina (Solis et al) [17]	Batch	180 (time 30 min)	72	55	—	—	—
Modified SBA–15 (Tucker et al) [18]	Continuous	130	80	70	0.5	6.34×10^{-5}	1.52×10^{-3}
ASB (this work)	Continuous	90	95	73	2.0	2.97×10^{-4}	0.20

[a] Fructose conversion was calculated as moles of fructose reacted per mole of fructose–fed.
[b] 5–HMF selectivity was calculated as moles of 5–HMF produced per mole of fructose reacted.
[c] LHSV was calculated as volumetric flow rate per unit weight of catalyst loaded in the reactor.
[d] Reaction rate was calculated as molar flow fed multiplied by conversion fraction per unit weight of catalyst loaded in the reactor.
[e] TOF was calculated as reaction rate per number of active sites.

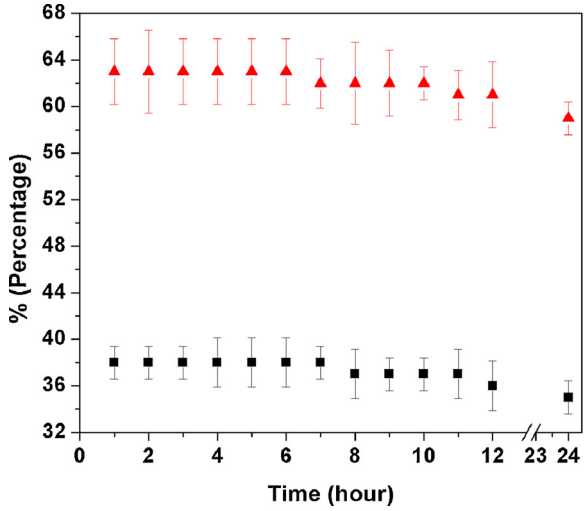

Fig. 7. Stability tests of ASB catalyst during 24 h of continuous reaction at 70 °C. Fructose conversion (squares) and selectivity towards 5–HMF (triangles).

remove impurities used during bi–functionalization is greater. Moreover, the thiol groups that were not grafted by sulfonic groups may also be removed during this change. It is therefore assumed there is a decrease in the percentage of grafted groups. Similarly, for ASB catalysts used, it may once again confirm the stability thereof, since, after 12 and 24 h of continuous reaction, no large losses of grafted groups were observed, which is evident from the measured sulfur content after reaction process. After 12 h of reaction, 88.1% of the groups were grafted to the catalyst, while after 24 h just 84.7% were grafted.

Table 4
Content of sulfur in the catalysts.

Catalysts		Sulfur concentration (wt. %)		Grafted (%)[c]
		Calculated[a]	Measured[b]	
Fresh	ASF	5.26	3.45	65.6
	ASB	9.49	5.02	52.9
Spent	ASB–12 h	5.02	4.42	88.1
	ASB–24 h	5.02	4.25	84.7

[a] Calculated by stoichiometric ratio.
[b] Measured by elementary analysis of sulfur.
[c] Calculated as: calculated value divided by measured value and then multiplied by 100.

3.9. DNP–enhanced solid–state CPMAS NMR spectroscopy

The DNP–enhanced ^{1}H–^{29}Si CPMAS NMR spectra shown in Fig. 9 (the second and third rows) confirm the binding structures of the grafted, hydrophilic functional groups that are tethered on the surface of the support (the first row). The second and third rows show DNP–enhanced ^{1}H–^{29}Si CPMAS spectra acquired under hydrophilic (AMUPol in 78% DMSO–d_6, 14% D_2O, and 8% H_2O) and hydrophobic (TEKPol in 90% TCE and 10% DMSO–d_6) conditions, respectively. As can be seen in Fig. 9, the catalysts exhibit the characteristics of the tertiary silicon bonds. Both the fresh and used catalysts exhibit ^{29}Si NMR signals at –75 and –55 ppm that correspond to T^3 and T^2 environments, respectively, to the silicon atom [15,16]. These spectral

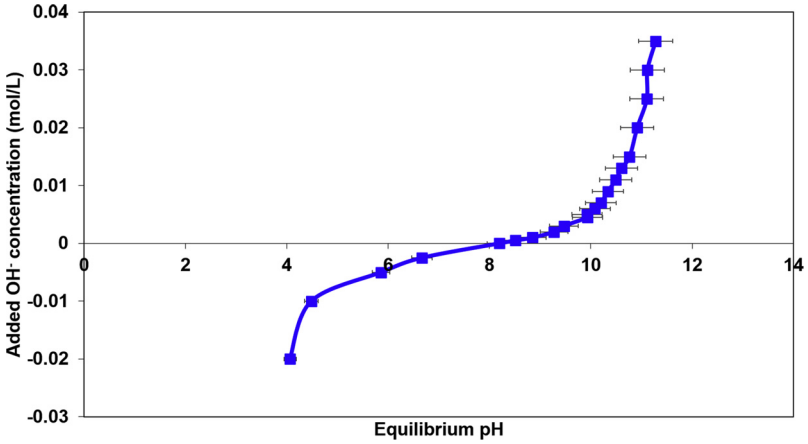

Fig. 8. Potentiometric titration of spent catalyst.

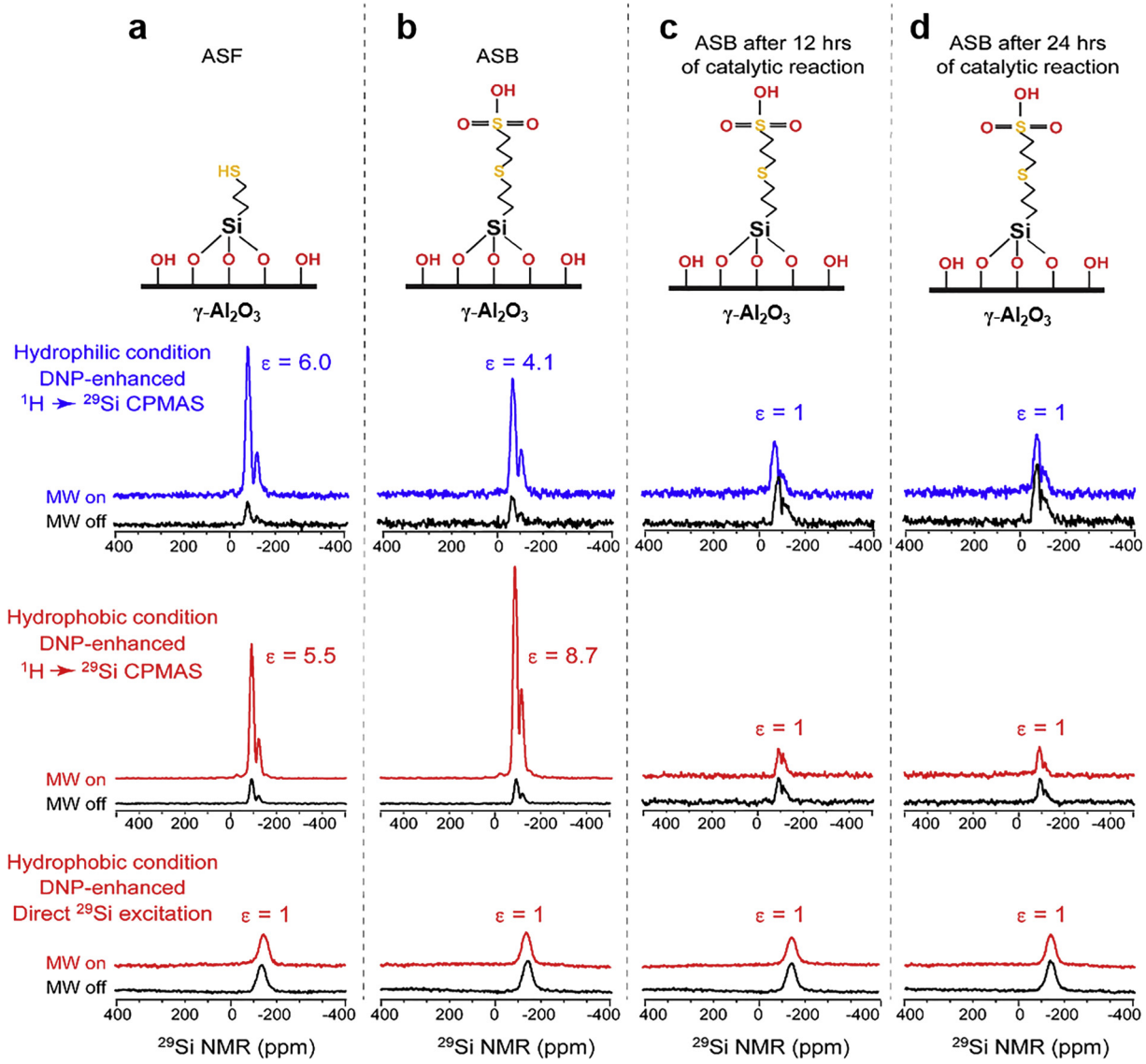

Fig. 9. DNP–enhanced ^{1}H–^{29}Si CPMAS (first and second row) and directly excited ^{29}Si MAS (third row) NMR spectra of: (a) fresh ASF catalyst, (b) fresh ASB catalyst, (c) ASB catalyst after 12 h of reaction and (d) ASB catalyst after 24 h of reaction. Both hydrophilic and hydrophobic environments were explored for DNP sampling conditions. DNP experiments were carried out at 100 K by adding 256 transients with a recycle time of 10 s.

results indicate that in each thiol group the silicon is bound to the surface of the alumina by means of two or three hydroxyl groups. Although these catalysts have the bonds T^2 and T^3, it is clear that in all cases there is a greater amount of type T^2 bonds (bonds with two hydroxyl groups) than T^3 bonds as we can decide based on their relative NMR peak intensities. The relative abundance of each T^n site depends on the modification technique [17].

When ^{1}H–^{29}Si CPMAS NMR spectra are acquired under the hydrophilic DNP sampling condition, a decrease in the ^{1}H–^{29}Si CPMAS signal intensity of ASB spectrum (Fig. 9b) was observed as compared to that of ASF sample (Fig. 9a) when the catalyst is not used. This would be due to an increase in the size of the functional group by the second functionalization that makes the resultant functional group in ASB with longer, hydrophobic $-CH_2CH_2–S-CH_2CH_2–$ chain before the terminal sulfonic acid. Then, an inefficient CP signal transfer effect would be resulted in between the NMR detecting ^{29}Si nuclei and the hydrogen atoms in water molecules in DNP juice that experience a signal enhancement effect from the electrons in biradicals by the DNP cross–effect [46,47]. This is because the longer, hydrophobic chains in the functional groups hinder water molecules from approaching closer to the Si atoms, resulting in longer ^{1}H(water)–^{29}Si dipolar coupling interactions and thus a decrease in the efficiency for ^{1}H–^{29}Si CP transfer. Also, the washing and heat treatments which were imposed on the catalytic sample during the synthesis step might have removed some thiol groups, which were weakly anchored on the surface. Under the hydrophobic DNP sampling condition (the third row in Fig. 9), however, the observed trend is the opposite that the signal intensity observed in the DNP–enhanced ^{1}H–^{29}Si CPMAS spectrum of ASB is actually stronger than that of ASF. In this case the polarities of the DNP–enhanced, hydrophobic TCE in DNP juice and the hydrophobic $-CH_2CH_2–S-CH_2CH_2–$ chain in the functional group are matched, resulting in TCEs' closer approach to ^{29}Si atoms in the functional groups.

When ^{29}Si MAS spectrum of each sample was acquired directly under microwave irradiation, no DNP enhancement effect was observed regardless of the type of the sampling conditions. These spectra also do not have enough spectral resolution to distinguish the T^2 and T^3 structures (the bottom row of Fig. 9). As in the case of those directly excited ^{29}Si MAS spectra in which no DNP effect was seen in all cases measured at both sampling conditions, when the catalytic reaction was

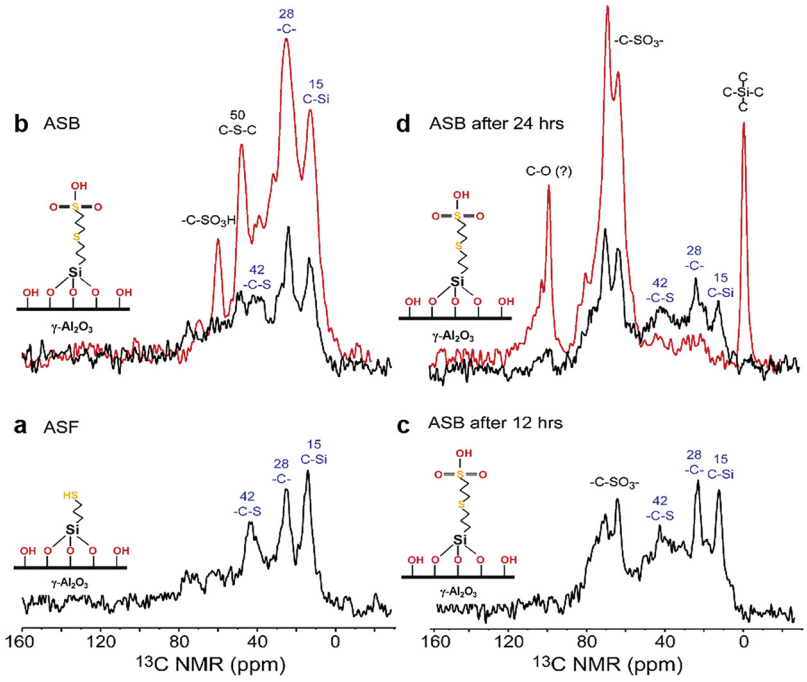

Fig. 10. ^{1}H–^{13}C CPMAS NMR spectra of: (a) fresh ASF catalyst, (b) fresh ASB catalyst, (c) ASB catalyst after 12 h of reaction and (d) ASB catalyst after 24 h of reaction. For (b) and (d) DNP–enhanced ^{1}H–^{13}C CPMAS spectra (red spectra) were additionally shown that were acquired under a hydrophilic DNP sampling condition (the same as in Fig. 9). Each conventional ^{1}H–^{13}C CPMAS spectrum measured at the room temperature required 26,000 scans while each DNP–enhanced one required only 256 scans. The signal enhancement factors of the DNP–enhanced spectra were about $\varepsilon = 40 \sim 45$. Spectra measured at 100 K with no microwave irradiation were not shown (For interpretation of the references to colour in this figure legend, the reader is referred to the web version of this article).

proceeded and lasts for more than 12 h, the DNP enhancing effect is lost even in the ^{1}H–^{29}Si CPMAS spectra obtained in both hydrophilic and hydrophobic DNP sampling conditions. During the use of a catalyst for reactions for 12 and 24 h, some amount of thiol groups would have been degraded from the catalytic surface, leaving only those that were strongly anchored as is validated by what was raised during the results of the elemental analysis. It is also important to note that after continuous catalytic reaction the T^{3} species are decreased in their concentration, which means that by the reaction conditions this form of bond is entrained or leached from the support. In general, however, it was observed that even after 24 h of catalytic reactions the functional groups were remained anchored to the support, albeit at a lower concentration.

These explanations however still do not validate the disappearance of the DNP enhancement effect in the ^{1}H–^{29}Si spectra for both sampling conditions measured under microwave irradiation. This observation rather suggests that the accessibility of the ^{1}H–containing solvent molecules, such as H_2O or TCE, in DNP juice to the grafted ^{29}Si atoms is hindered, indicating that, as the reaction progresses, the Si atoms on the surface of the catalyst are covered by molecules or molecular fragments formed during catalytic reactions. Another possibility is that the structure of the C—Si—C sites in the functional groups might be modified, separating them away from the outer surface of the catalyst. This phenomenon is believed to occur if the grafted functional groups on the surface of the catalyst are modified or just buried by the adsorption of a small amount of the reactants, products or intermediates produced during the catalytic reaction [47,48]. Because the amount of these molecules accumulated on the catalytic surface is low, they are hard to be detected in the conventional ^{1}H–^{29}Si CPMAS spectroscopy but are readily visible in the DNP–enhanced ^{1}H–^{29}Si CPMAS spectroscopy that is specialized in surface analysis. Thus, DNP–enhanced ^{1}H–^{29}Si and ^{1}H–^{13}C (*vide infra*) CPMAS methods would be an adequate surface–enhanced spectroscopy (SENS) to monitor the structural changes on catalytic surfaces with a great sensitivity.

DNP–enhanced ^{1}H–^{13}C CPMAS NMR spectra measured under the hydrophilic condition (20 mg sample + 20 μL of 5 mM TOTAPOL in 90% D_2O and 10% H_2O) allowed to follow the functionalization of the thiol group and the bi–functionalization of the sulfonic acid group. This mode of measurements confirms that the anchoring of the groups was successful, demonstrates that the structure of functional groups was grafted on alumina catalyst, and verifies that these groups were kept after the reaction. In addition, the measured spectra verify the hypothesis made previously in Fig. 9 that exhibited are additional ^{13}C peaks from unknown chemical species that would be adsorbed and accumulated on the catalyst surface as the reaction underwent. Fig. 10 shows the NMR results of the modified alumina catalysts before and after the reaction measured at an ambient temperature. Additionally, shown in (b) and (d) in red lines are the DNP–enhanced ^{1}H–^{13}C CPMAS NMR spectra of ASB measured at 100 K before (b) and after (d) being used for catalytic reaction for 24 h. Note the relative signal gains resulted in from the DNP–enhanced CPMAS spectra measured at 100 K with respect to the conventional CPMAS spectra measured at an ambient temperature that only 256 scans were utilized for obtaining DNP–enhanced spectra while as many as 26,000 scans were utilized for obtaining those conventional spectra. The signals at 15 ppm (C–Si) is related to carbon, which is directly linked to silicon (–Si − CH_2–). The signal at 28 ppm (–C–) confirms the incorporation of the sulfonic group (− CH_2 − CH_2–S − CH_2 − CH_2–) and 50 ppm (—C–S–C–) is related to the thiol group (− CH_2–S − CH_2–). Finally, the signal at ~ 60 ppm (–C–S) is related to the carbon bound to the sulfonic group (− CH_2–SO_3H) [15,17,18]. The structure of the grafted catalyst is shown on the left side of each spectrum in Fig. 10. The spectra of Fig. 10c and d show that after the reaction some types of deactivation in the catalyst occurred by the entrainment, leaching, or degradation of the groups. In addition, degradation or adsorption and accumulations of some unknown chemical species on the surface are confirmed in Fig. 10d. Those additional peaks in Fig. 10d may correspond to $(–C)_4$–Si and C—O moieties according to the chemical shift positions of the peaks. The presence of $(–C)_4$–Si moiety evidences a structural modification occurred on the Si site. As was discussed in Fig. 9, not only the structurally modified functional groups but chemical species adsorbed and accumulated on the catalytic surface would bury Si sites into inner layers, screening them from the approach of the proton–containing solvent molecules in DNP juice [49–51]. The amount of these species modified or adsorbed on the surface would be scarce as these species were not effectively detected in the conventional CPMAS spectrum as shown in (d). However, the DNP–enhanced ^{1}H–^{13}C CPMAS method was proven that it was sensitive enough to detect structural changes on catalytic surfaces. Still, it also shows that after 24 h continuously the catalyst kept an efficient stability and the groups remained anchored thereto.

4. Conclusions

This work shows that was possible to obtain novel catalyst as synthetic alumina support by the sol–gel method, which was a better support than commercial alumina, due to its high contents of O—H groups and great superficial area. The modification of the catalyst was confirmed by the presence of thiol and sulfonic groups by FTIR. The formation of the reaction product was evidenced by FTIR, observing that the increase in concentration of 5-HMF in solution by action of the reaction temperature produces the increase of the band at 1648 cm^{-1} due to C═O vibrations stretching of the aldehyde group in the 5–HMF and at 1522 cm^{-1} due to C═C stretching vibrations of 5–HMF ring. For the system, it was observed that the conversion of fructose and the selectivity to 5–HMF were higher as reaction temperature increases, obtaining values of 95 and 73% at 90 °C respectively. The modified catalyst showed no loss in activity during 24 h of continuous reaction at 70 °C. However, it was observed that the loss of sulfur content was 15% at these conditions by elemental analysis, which shows a better stability of the catalyst compared with previous works as shown in Table 3. Moreover, the yield in the conversion of fructose and the selectivity to 5–HMF did not undergo significant changes (less than 5%). This was also confirmed by NMR and DNP NMR, where it was observed that the thiol and sulfonic groups remained anchored to the catalyst after 12 and 24 h of reaction although the grafted functional groups on the catalytic surface might be buried by the adsorption and accumulation of molecules formed during the catalytic reactions. Finally, in the field of catalytic reactions in which wastes are converted to useful products, the ASB catalyst presents a potential to be used in the continuous processes of 5–HMF production.

Acknowledgments

This work was funded under No. 02–084347–PST–14/105 by Facultad de Ciencias Químicas, Universidad Autónoma de Nuevo León (UANL), México; and was supported by government institutions as the “Consejo Nacional de Ciencia y Tecnología (CONACyT)” from Mexico for a scholarship. A portion of this work was performed at the National High Magnetic Field Laboratory, which is supported by National Science Foundation Cooperative Agreement No. DMR–1157490, DMR–1644779, and the State of Florida. The MAS-DNP system at the NHMFL is funded in part by NIH S10 OD018519 (magnet and console), and NSF CHE-1229170 (gyrotron).

References

[1] S.V. Mohan, G.N. Nikhil, P. Chiranjeevi, C.N. Reddy, M.V. Rohit, A.N. Kumar, O. Sarkar, Waste biorefinery models towards sustainable circular bioeconomy: Critical review and future perspectives, Bioresour. Technol. 215 (2016) 2–12.
[2] J. Sadhukhan, E. Martinez–Hernandez, R.J. Murphy, D.K.S. Ng, M.H. Hassim, K.S. Ng, W.Y. Kin, I.F.M. Jaye, M.Y.L.P. Hang, V. Andiappan, Role of bioenergy, biorefinery and bioeconomy in sustainable development: Strategic pathways for Malaysia, Renewable Sustainable Energy Rev. 81 (2018) 1966–1987.
[3] A.A. Koutinas, A. Vlysidis, D. Pleissner, N. Kopsahelis, I. Lopez Garcia, I.K. Kookos, S. Papanikolaou, T.H. Kwan, C.S.K. Lin, Valorization of industrial waste and by—product streams via fermentation for the production of chemicals and biopolymers, Chem. Soc. Rev. 43 (2014) 2587–2627.
[4] I.K.M. Yu, D.C.W. Tsang, A.C.K. Yip, S.S. Chen, Y.S. Ok, C.S. Poon, Valorization of food waste into hydroxymethylfurfural: Dual role of metal ions in successive conversion steps, Bioresour. Technol. 219 (2016) 338–347.
[5] S.S. Chen, T. Maneerung, D.C.W. Tsang, Y.S. Ok, C.–H. Wang, Valorization of biomass to hydroxymethylfurfural, levulinic acid, and fatty acid methyl ester by heterogeneous catalysts, Chem. Eng. J. 328 (2017) 246–273.
[6] I.K.M. Yu, K.L. Ong, D.C.W. Tsang, M.A. Haque, T.H. Kwan, S.S. Chen, K. Uisan, S. Kulkarni, C.S.K. Lin, Chemical transformation of food and beverage waste–derived fructose to hydroxymethylfurfural as a value–added product, Catal. Today (2018).
[7] J.M. Thomas, J.C. Hernandez–Garrido, R.G. Bell, A General Strategy for the Design of New Solid Catalysts for Environmentally Benign Conversions, Top. Catal. 52 (2009) 1630–1639.
[8] J. Sanchez–Valente, X. Bokhimi, J.A. Toledo, Synthesis and catalytic properties of nanostructured aluminas obtained by sol–gel method, Appl. Catal. A Gen. 264 (2004) 175–181.
[9] K. Sohlberg, S.J. Pennycook, S.T. Pantelides, Explanation of the observed dearth of three–Coordinated Al on γ–Alumina surfaces, J. Am. Chem. Soc. 121 (1999) 10999–11001.
[10] S. Bertazzo, K. Rezwan, Control of α–Alumina surface charge with carboxylic acids, Langmuir 26 (2010) 3364–3371.
[11] T. Wang, Catalytic Conversion of Glucose to 5–hydroxymethylfurfural As a Potential Biorenewable Platform Chemical, (2014).
[12] A. Mukherjee, M.–J. Dumont, V. Raghavan, Review: Sustainable production of hydroxymethylfurfural and levulinic acid: Challenges and opportunities, Biomass Bioenergy 72 (2015) 143–183.
[13] D.M. Alonso, S.H. Hakim, S. Zhou, W. Won, O. Hosseinaei, J. Tao, V. Garcia–Negron, A.H. Motagamwala, M.A. Mellmer, K. Huang, C.J. Houtman, N. Labbé, D.P. Harper, C.T. Maravelias, T. Runge, J.A. Dumesic, Increasing the revenue from lignocellulosic biomass: maximizing feedstock utilization, Sci. Adv. 3 (2017).
[14] F. Shahangi, A. Chermahini, M. Saraji, Dehydration of fructose and glucose to 5–hydroxymethylfurfural over Al-KCC-1 silica, J. Energy Chem. 27 (2018) 769–780.
[15] C. Bispo, K. De Oliveira Vigier, M. Sardo, N. Bion, L. Mafra, P. Ferreira, F. Jérôme, Catalytic dehydration of fructose to HMF over sulfonic acid functionalized periodic mesoporous organosilicas: role of the acid density, Catal. Sci. Technol. 4 (2014) 2235–2240.
[16] A.J. Crisci, M.H. Tucker, J.A. Dumesic, S.L. Scott, Bifunctional Solid Catalysts for the Selective Conversion of Fructose to 5–Hydroxymethylfurfural, Top. Catal. 53 (2010) 1185–1192.
[17] C. Solis Maldonado, J. Rivera De la Rosa, C.J. Lucio–Ortiz, J.S. Valente, M.J. Castaldi, Synthesis and characterization of functionalized alumina catalysts with thiol and sulfonic groups and their performance in producing 5–hydroxymethylfurfural from fructose, Fuel 198 (2017) 134–144.
[18] M.H. Tucker, A.J. Crisci, B. Wigington, N. Phadke, R. Alamillo, J. Zhang, S.L. Scott, J.A. Dumesic, Acid–Functionalized SBA–15–Type Periodic Mesoporous Organosilicas and their Use in the Continuous Production of 5–Hydroxymethylfurfural, ACS Catal. (2012) 1865–1876.
[19] C.V. McNeff, D.T. Nowlan, L.C. McNeff, B. Yan, R.L. Fedie, Continuous production of 5–hydroxymethylfurfural from simple and complex carbohydrates, Appl. Catal. A Gen. 384 (2010) 65–69.
[20] P. Rivalier, J. Duhamet, C. MoreaRiveru, R. Durand, Development of a continuous catalytic heterogeneous column reactor with simultaneous extraction of an intermediate product by an organic solvent circulating in countercurrent manner with the aqueous phase, Catal. Today 24 (1995) 165–171.
[21] C. Moreau, R. Durand, S. Razigade, J. Duhamet, P. Faugeras, P. Rivalier, P. Ros, G. Avignon, Dehydration of fructose to 5–hydroxymethylfurfural over H–mordenites, Appl. Catal. A Gen. 145 (1996) 211–224.
[22] P. Carniti, A. Gervasini, S. Biella, A. Auroux, Niobic acid and niobium phosphate as highly acidic viable catalysts in aqueous medium: fructose dehydration reaction, Catal. Today 118 (2006) 373–378.
[23] P. Carniti, A. Gervasini, M. Marzo, Silica–niobia oxides as viable acid catalysts in water: Effective vs. intrinsic acidity, Catal. Today 152 (2010) 42–47.
[24] M. Zhang, K. Su, H. Song, Z. Li, B. Cheng, The excellent performance of amorphous Cr_2O_3, SnO_2, SrO and graphene oxide–ferric oxide in glucose conversion into 5–HMF, Catal. Commun. 69 (2015) 76–80.
[25] M.H. Tucker, R. Alamillo, A.J. Crisci, G.M. Gonzalez, S.L. Scott, J.A. Dumesic, Sustainable solvent systems for use in tandem carbohydrate dehydration hydrogenation, ACS sustain, Chem. Eng. 1 (2013) 554–560.
[26] Y. Roman–Leshkov, J.A. Dumesic, Solvent effects on fructose dehydration to 5–hydroxymethylfurfural in biphasic systems saturated with inorganic salts, Top. Catal. 52 (2009) 297–303.
[27] T.K. Phung, A. Lagazzo, M.A. Rivero Crespo, V. Sanchez Escribano, G. Busca, A study of commercial transition aluminas and of their catalytic activity in the dehydration of ethanol, J. Catal. 311 (2014) 102–113.
[28] Z. Shi, W. Jiao, L. Chen, P. Wu, Y. Wang, M. He, Clean synthesis of hierarchically structured boehmite and gamma–alumina with a flower–like morphology, Microporous Mesoporous Mater. 224 (2016) 253–261.
[29] X. Song, P. Qu, H. Yang, X. He, G. Qiu, Synthesis of γ–Al_2O_3 nanoparticles by chemical precipitation method, J. Cent. South Univ. Technol. 12 (2005) 536–541.
[30] N. Suzuki, Y. Yamauchi, One–step synthesis of hierarchical porous γ–alumina with high surface area, J. Solgel Sci. Technol. 53 (2010) 428–433.
[31] D. Yang, B. Paul, W. Xu, Y. Yuan, E. Liu, X. Ke, R.M. Wellard, C. Guo, Y. Xu, Y. Sun, H. Zhu, Alumina nanofibers grafted with functional groups: a new design in efficient sorbents for removal of toxic contaminants from water, Water Res. 44 (2010) 741–750.
[32] M.H. Marchena, M. Granada, A.V. Bordoni, M. Joselevich, H. Troiani, F.J. Williams, A. Wolosiuk, Organized thiol functional groups in mesoporous core shell colloids, J. Solid State Chem. 187 (2012) 97–102.
[33] J. Mosa, A. Durán, M. Aparicio, Sulfonic acid–functionalized hybrid organic–inorganic proton exchange membranes synthesized by sol–gel using 3–mercaptopropyl trimethoxysilane (MPTMS), J. Power Sources 297 (2015) 208–216.
[34] R.J. Kalbasi, A.R. Massah, B. Daneshvarnejad, Preparation and characterization of bentonite/PS–SO_3H nanocomposites as an efficient acid catalyst for the Biginelli reaction, Appl. Clay Sci. 55 (2012) 1–9.
[35] B. Greenhalgh, M. Fee, A. Dobri, J. Moir, R. Burich, J.–P. Charland, M. Stanciulescu, $DeNO_x$ activity–TPD correlations of NH_3–SCR catalysts, J. Mol. Catal. A Chem. 333 (2010) 121–127.
[36] C.V. Loricera, P. Castano, A. Infantes–Molina, I. Hita, A. Gutierrez, J.M. Arandes, J.L.G. Fierro, B. Pawelec, Designing supported ZnNi catalysts for the removal of oxygen from bio–liquids and aromatics from diesel, Green Chem. 14 (2012)

2759–2770.
[37] J.Z. Hu, S. Xu, J.H. Kwak, M.Y. Hu, C. Wan, Z. Zhao, J. Szanyi, X. Bao, X. Han, Y. Wang, C.H.F. Peden, High field ^{27}Al MAS NMR and TPD studies of active sites in ethanol dehydration using thermally treated transitional aluminas as catalysts, J. Catal. 336 (2016) 85–93.
[38] K.S.W. Sing, Reporting physisorption data for gas/solid systems with special reference to the determination of surface area and porosity, Pure Appl. Chem. 54 (1982) 2201.
[39] G. Leofanti, M. Padovan, G. Tozzola, B. Venturelli, Surface area and pore texture of catalysts, Catal. Today 41 (1998) 207–219.
[40] M. Sánchez–Cárdenas, J. Medina–Valtierra, S.–K. Kamaraj, F. Trejo–Zárraga, L. Antonio Sánchez–Olmos, Physicochemical effect of Pt nanoparticles/γ–Al_2O_3 on the oleic acid hydrodeoxygenation to biofuel, Environ. Prog. Sustain. Energy 36 (2017) 1224–1233.
[41] M. del P. Buera, J. Chirife, S.L. Resnik, R.D. Lozano, Nonenzymatic browning in liquid model systems of high water activity: kinetics of color changes due to caramelization of various single sugars, J. Food Sci. 52 (1987) 1059–1062.
[42] M. del P. Buera, J. Chirife, S.L. Resnik, G. Wetzler, Nonenzymatic browning in liquid model systems of high water activity: kinetics of color changes due to Maillard's reaction between different single sugars and glycine and comparison with caramelization browning, J. Food Sci. 52 (1987) 1063–1067.
[43] N. Romano, M. Santos, P. Mobili, R. Vega, A. Gómez–Zavaglia, Effect of sucrose concentration on the composition of enzymatically synthesized short–chain fructo–oligosaccharides as determined by FTIR and multivariate analysis, Food Chem. 202 (2016) 467–475.
[44] D.D. Purkayastha, V. Madhurima, Interactions in water–THF binary mixture by contact angle, FTIR and dielectric studies, J. Mol. Liq. 187 (2013) 54–57.
[45] M. Ozawa, M. Hattori, Ultrasonic vibration potential and point of zero charge of some rare earth oxides in water, J. Alloys Compd. 408–412 (2006) 560–562.
[46] A.V. Kessenikh, V.I. Lushchikov, A.A. Manenkov, Y.V. Taran, Magnetization behavior of a copper–cadmium ferrite in pulsed fields up to 200 KOE, Sov. Phys. Solid State. 5 (1963) 321.
[47] A.V. Kessenikh, A.A. Manenkov, G.I. Pyatnitskii, Polarization reversal characteristics of ammonium hydrogen sulfate $(NH_4)HSO_4$, Sov. Phys. Solid State. 6 (1964) 641.
[48] C.F. Hwang, D.A. Hill, Phenomenological model for the new effect in dynamic polarization, Phys. Rev. Lett. 19 (1967) 1011–1014.
[49] Q. Yang, M.P. Kapoor, S. Inagaki, Sulfuric acid–Functionalized mesoporous benzene − Silica with a molecular–Scale periodicity in the walls, J. Am. Chem. Soc. 124 (2002) 9694–9695.
[50] W.–C. Liao, B. Ghaffari, C.P. Gordon, J. Xu, C. Copéret, Dynamic nuclear polarization surface enhanced (NMR) spectroscopy (DNP SENS): principles, protocols, and practice, Curr. Opin. Colloid Interface Sci. (2018).
[51] J. van Bentum, B. van Meerten, M. Sharma, A. Kentgens, Perspectives on DNP–enhanced NMR spectroscopy in solutions, J. Magn. Reson. 264 (2016) 59–67.